*Geophys. J. Int.* (1999) **139,** 283–295

# Modelling coseismic displacements during the 1997 Umbria–Marche earthquake (central Italy)

Ingrid Hunstad,[1] Marco Anzidei,[1] Massimo Cocco,[1] Paolo Baldi,[2] Alessandro Galvani[1] and Arianna Pesci[1]

[1] *Istituto Nazionale di Geofisica, Via di Vigna Murata* 605, 00143, *Rome, Italy. E-mail: hunstad@nettuno.ingrm.it*
[2] *Dipartimento di Fisica, Settore di Geofisica, Università di Bologna, Viale Berti Pichat* 8, 40127, *Bologna, Italy*

Accepted 1999 May 26. Received 1999 May 26; in original form 1998 June 24

## SUMMARY

We propose a dislocation model for the two normal faulting earthquakes that struck the central Apennines (Umbria–Marche, Italy) on 1997 September 26 at 00:33 ($M_w$ 5.7) and 09:40 GMT ($M_w$ 6.0). We fit coseismic horizontal and vertical displacements resulting from GPS measurements at several monuments of the IGMI (Istituto Geografico Militare Italiano) by means of a dislocation model in an elastic, homogeneous, isotropic half-space. Our best-fitting model consists of two normal faults whose mechanisms and seismic moments have been taken from CMT solutions; it is consistent with other seismological and geophysical observations. The first fault, which is 6 km long and 7 km wide, ruptured during the 00:33 event with a unilateral rupture towards the SE and an average slip of 27 cm. The second fault is 12 km long and 10 km wide, and ruptured during the 09:40 event with a nearly unilateral rupture towards the NW. Slip distribution on this second fault is non-uniform and is concentrated in its SE portion (maximum slip is 65 cm), where rupture initiated. The 00:33 fault is deeper than the 09:40 one: the top of the first rupture is deeper than 1.7 km; the top of the second is 0.6 km deep. In order to interpret the observed epicentral subsidence we have also considered the contributions of two further moderate-magnitude earthquakes that occurred on 1997 October 3 ($M_w$ 5.2) and 6 ($M_w$ 5.4), immediately before the GPS survey, and were located very close to the 09:40 event of September 26. We compare the pattern of vertical displacements resulting from our forward modelling of GPS data with that derived from SAR interferograms: the fit to SAR data is very good, confirming the reliability of the proposed dislocation model.

**Key words:** central Apennines, coseismic displacements, GPS data, normal faulting.

## INTRODUCTION

Two earthquakes struck the central Apennines (Umbria–Marche, Italy) on 1997 September 26 at 00:33 GMT ($M_w$ 5.7) and 09:40 GMT ($M_w$ 6.0) (see Fig. 1); they caused severe damages and several casualties. In the surrounding area several moderate-magnitude historical earthquakes (Boschi *et al.* 1995; Amato *et al.* 1998) occurred in the past few centuries (see Fig. 2). The two closest and most recent seismic events occurred near Norcia in 1979 ($M_S$ 5.8, Deschamps *et al.* 1984) and near Gubbio in 1984 ($M_S$ 5.3, Haessler *et al.* 1988) and both ruptured normal faults as shown in Fig. 1. The September 1997 earthquakes and their aftershocks have been recorded by both permanent and temporary seismic stations, which allowed earthquake locations to be found and the analysis of the seismic sequence (Amato *et al.* 1998), as well as the computation of CMT fault plane solutions (Ekström *et al.* 1998). Several $M \geq 4.0$ aftershocks occurred in the following 50 days. On October 14 (at 15:23 GMT) another moderate earthquake ($M_w$ 5.5) occurred 15 km south of the epicentral area of the September 26 events, extending the whole seismogenic area towards the SE (see Fig. 1). The CMT fault plane solutions of the three largest events of the sequence and of the two largest aftershocks, which occurred very close to the September 26 main-shock hypocentres, are shown in Fig. 1. Fig. 2 depicts the tectonic setting and the historical earthquakes that occurred in this central section of the Apennines. An extensional tectonic stress field is suggested by fault plane solutions of recent earthquakes (shown in Fig. 1).

The aim of this paper is to constrain a dislocation model for the two largest earthquakes of September 26 ($M_w$ 5.7 and 6.0) using geodetic data. Up to now only vertical displacements (from levelling measurements) have been used to study earthquakes in Italy such as the 1908 Messina ($M$7.3) and the 1915

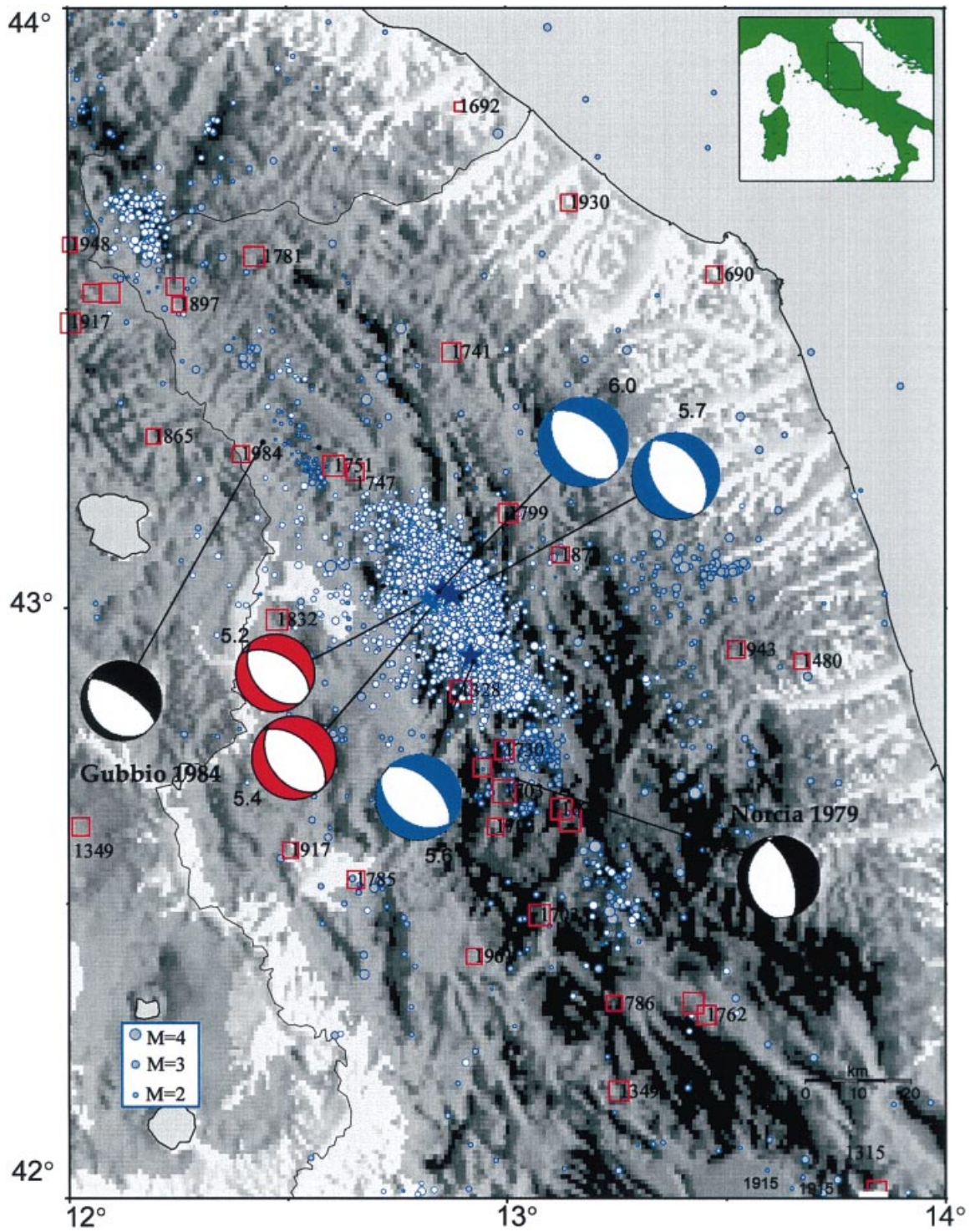


**Figure 1.** Instrumental seismicity and aftershock distribution during the 1997 Umbria–Marche sequence (September–November 1998). Open squares show historical earthquakes. Focal mechanisms of the three largest-magnitude events of the sequence (September 26 00:33 GMT $M_w$ 5.7, 09:40 $M_w$ 6.0 and October 14 $M_w$ 5.6) are shown in blue, while those of the two largest aftershocks (October 3 $M_w$ 5.2 and October 6 $M_w$ 5.4) are indicated in red. The two closest and most recent earthquakes (the 1979 Valnerina and 1984 Gubbio events) and their focal mechanisms are also shown on the map. An extensional tectonic setting is revealed by fault plane solutions of recent earthquakes, suggesting that the present-day active stress field is characterized by nearly horizontal extension perpendicular to the Apenninic belt.

Avezzano ($M$6.5) seismic events (Capuano *et al.* 1988; Ward & Valensise 1989; De Natale & Pingue 1991) as well as the 1980 Irpinia ($M$6.9) earthquake (Bernard & Zollo 1989; Pantosti & Valensise 1990; Pingue & De Natale 1993) . Only recently have the Istituto Geografico Militare Italiano (IGMI) and other Italian institutions deployed GPS networks for cartographical purposes or for monitoring the crustal deformation of seismic areas. In this study we analyse GPS measurements collected

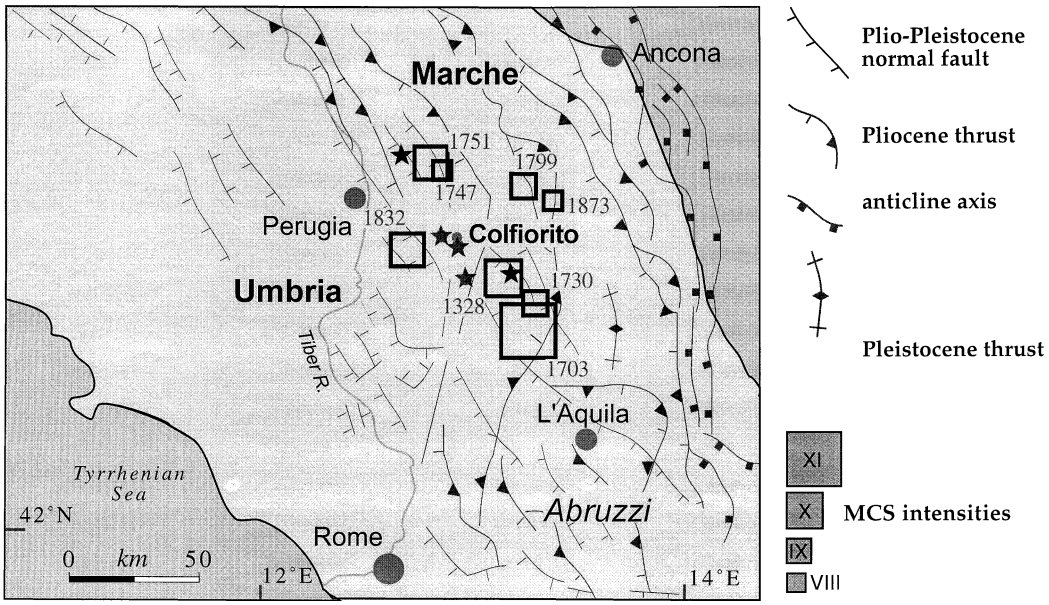


**Figure 2.** Structural setting of the Umbria–Marche region. The main historical earthquakes are shown by open squares, while the stars indicate the three largest events of the 1997 sequence.

during two campaigns performed in 1992–1996 by the IGMI and in 1997 by the Istituto Nazionale di Geofisica (ING) immediately after the two earthquakes of September 26. This data set is particularly relevant because for the first time in Italy coseismic horizontal displacements have been measured and used to constrain a source model.

## GPS DATA

During the period 1992–1996, the IGMI set up and measured a new national geodetic network designed for GPS observations consisting of more than 1200 sites uniformly distributed over the Italian peninsula and the islands. The average accuracy of the coordinates of each GPS monument is estimated by the IGMI to be 2.2 cm for the horizontal components and 3.5 cm for the vertical component, all at 95 per cent confidence levels (Surace 1993, 1997).

10 days after the two September 26 events, we began to reoccupy the monuments from the IGMI network (Fig. 3) within 30 km of the epicentre using Trimble 4000SSE/SSI dual-frequency GPS receivers. 12 sites were occupied twice for 4–6 hr measurement sessions. Two of them (FOLI and COLF) were occupied continuously during the campaign. The 1997 GPS observations were processed with the Bernese software (version 4.0, Rothacher & Mervart 1996) using the precise satellite ephemerides computed at the Centre for Orbit Determination in Europe (CODE), adopting standard procedures: tropospheric delays were estimated and the ambiguities were fixed, rounding their real values to the nearest integer values using variance and covariance information (Rothacher & Mervart 1996). The solutions of independent baselines were adjusted in a network; 3-D coordinates were obtained at a mean accuracy of 1.0 cm in the horizontal components (mean value of the semi-axes of the error ellipses) and 2.0 cm in the vertical component, both at 95 per cent confidence levels (see Fig. 3 and Table 1). The mean values of the rms GPS baseline Cartesian components are equal to 0.9, 0.5 and 0.8 cm in the $x$-, $y$- and $z$-components, respectively.

**Table 1.** Planar and vertical accuracy of the ING97 and IGM95 GPS campaigns. *S*max and *S*min are the major and minor semi-axes of the error ellipses (planar component); *D*h is the vertical accuracy (all at 95 per cent confidence levels).

| Station | *S*max (mm) | *S*min (mm) | Az. | *D*h (mm) |
|---|---|---|---|---|
| 01–COLF | 5.4 | 5.4 | 11.25 | 11.9 |
| 02–BEVA | 9.5 | 6.7 | 01.35 | 19.2 |
| 03–CROC | 12.2 | 9.5 | 06.51 | 23.4 |
| 04–CAPA | 10.8 | 8.1 | 07.48 | 19.2 |
| 05–CSAN | 14.8 | 10.8 | 00.23 | 30.1 |
| 06–FOLI | 6.7 | 5.4 | 06.53 | 13.5 |
| 07–GAIF | 10.8 | 8.1 | 00.56 | 20.3 |
| 08–OGAT | 5.9 | 4.0 | 01.34 | 10.4 |
| 09–PENN | 10.8 | 9.5 | 02.19 | 22.3 |
| 10–RIVO | 9.5 | 6.7 | 07.30 | 18.2 |
| 11–TPAR | 14.8 | 13.5 | 11.16 | 30.6 |
| 12–VISS | 12.2 | 9.5 | 17.10 | 29.0 |
| IGM95 mean accuracy | 22 | 22 | – | 35 |

In Table 2 the repeatabilities of the independent baselines used for network adjustment are reported (their residuals with respect to the adjustment values). The coseismic displacements were obtained by comparing the 1997 campaign coordinates with those collected by the IGMI for the study area in 1995; they are listed in Table 3 and shown in Fig. 3, together with an estimate of their error ellipses. Unfortunately, the displacement error ellipses are computed from the 1995 campaign, for which we cannot dispose of the covariance matrix relative to the adjustment of the IGMI network. For this reason, the displacement uncertainties and the error ellipses can be estimated only by using the average accuracy of the IGMI coordinates together with the accuracy derived by a rigorous adjustment of the observations performed in 1997. Some observations from the 1992–1996 IGMI survey were reprocessed to ensure an independent check for some baseline lengths of the

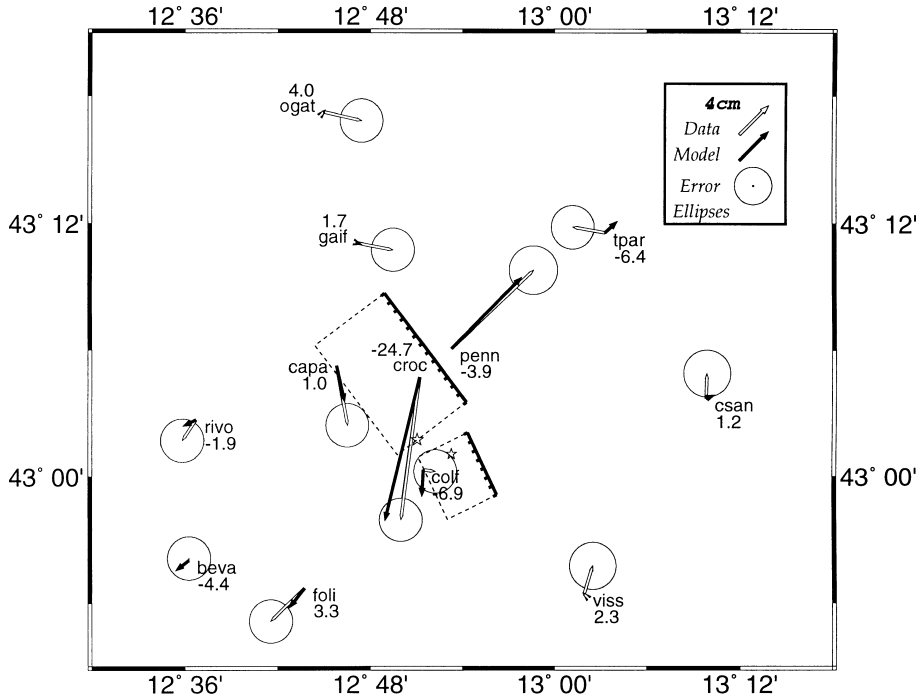


**Figure 3.** Map of the monuments of the GPS network used in this study. The epicentres of the two September 26 events are shown (stars). The error ellipses at 95 per cent confidence level of the displacement vectors are shown (for the 1995 campaign only, the IGM95 mean accuracy is available; see Table 1). Comparisons between observed GPS horizontal displacements (open arrows) and predicted displacements (solid arrows) resulting from the best-fitting model for the two 1997 September 26 earthquakes are also shown. Numbers indicate observed vertical displacements (units in cm) (see Table 3). The surface projections of the activated faults are shown as a line with ticks on the downthrown side.

network that cross the epicentral area: the baseline length scatter was less than 3 cm. In order to eliminate any systematic effect due to differences in reference frame, a seven-parameter conformal transformation has been applied, minimizing the coordinate residuals of the sites located at distances greater than 15 km from the epicentres. According to the accuracies of the network adjustment solution of the 1995 and 1997 GPS surveys (shown in Fig. 3 and listed in Tables 1 and 2), for our investigation we rely on the fit to those monuments where observed horizontal and vertical displacements are larger than 3.0 and 4.0 cm, respectively. This is quite a restrictive assumption, which allows us to avoid bias in modelling coseismic displacement possibly due to data processing.

The four closest sites (CROC, PENN, COLF, CAPA) to the fault and FOLI (see Fig. 3) provided the largest horizontal displacements. In performing our forward modelling we verify that the predictions of the coseismic displacements at the other monuments are below the uncertainties derived by the network adjustment. We exclude TPAR from our analysis because this monument was measured only during a single session because of instrument problems during the second survey session; therefore, it provided statistically unreliable final coordinates.

Our GPS measurements were performed 3 yr after the IGMI survey, so we have to take into account the contribution of tectonic deformation during this time interval. As the geodetic strain in the Umbria–Marche area over a period of 100 yr is no more than 0.1 ppm $yr^{-1}$, as recently computed by Hunstad & England (1999) using angle change data from repeated triangulation performed by the IGMI between 1870 and 1950, we can assume that the observed displacements are due to the earthquake dislocation. Moreover, the measured vertical displacements resulting from GPS data agree with those provided by differential SAR interferometry using pre- and post-seismic ERS satellite images spanning a period of 35 days (Stramondo *et al.* 1999); this provides further confirmation that the observed displacement is coseismic.

On October 14 a third moderate-magnitude ($M_w$ 5.6) earthquake occurred south of the September 26 epicentres (see Figs 1 and 2) in the area of Sellano and Preci. Two weeks after this event we reoccupied five new sites of the IGMI–GPS network and three sites of the former survey (VISS, FOLI and COLF in Fig. 3). Two were occupied continuously (FOLI and COLF), while the remainder were occupied for a single 8 hr session. The analysis of the GPS data from this further campaign did not provide significant detectable displacements (less than 2 cm for the planar component and 4 cm for the vertical component). We thus conclude that the Sellano earthquake did not produce measurable surface deformation at the reoccupied monuments, eliminating any possibility of performing a source modelling for this seismic event with GPS data.

## CONSTRAINTS ON FAULT GEOMETRY

In this study we present the results of a forward modelling of the horizontal and vertical GPS displacements caused by the two earthquakes of 1997 September 26. The available geodetic measurements do not allow us to attempt any inversion to determine fault geometry and slip distribution, but they can provide constraints on the faulting mechanism and slip amplitudes. Despite the small dimension of the available data set, the positions of some geodetic monuments are ideally

**Table 2.** Repeatability of the independent baselines used for network adjustment and their residuals with respect to the adjusted values.

| Baseline | Residual (m) |
|---|---|
| | DOY 280 |
| COLF–PERU | −0.003 |
| CROC–PERU | −0.001 |
| | DOY 281 |
| BEVA–CROC | −0.005 |
| COLF–CROC | −0.004 |
| CSAN–CROC | 0.005 |
| FOLI–CROC | −0.004 |
| GAIF–CROC | −0.009 |
| PERU–CROC | −0.007 |
| RIVO–CROC | −0.002 |
| VISS–CROC | 0.003 |
| | DOY 282 |
| BEVA–COLF | 0.001 |
| CAPA–COLF | −0.003 |
| CROC–COLF | 0.001 |
| CSAN–COLF | −0.001 |
| FOLI–COLF | −0.001 |
| OGAT–COLF | 0.003 |
| GAIF–COLF | 0.011 |
| PERU–COLF | 0.003 |
| PENN–COLF | 0.004 |
| RIVO–COLF | −0.001 |
| VISS–COLF | −0.001 |
| | DOY 283 |
| COLF–PERU | 0.001 |
| CAPA–PERU | −0.003 |
| CROC–PERU | 0.001 |
| GAIF–PERU | 0.009 |
| PENN–PERU | −0.007 |
| TPAR–PERU | −0.003 |
| | DOY 284 |
| COLF–CROC | 0.005 |
| PERU–CROC | 0.001 |

located with respect to the activated faults (Fig. 3). The surface projection of the fault plane of the second shock (Amato *et al.* 1998; Ekström *et al.* 1998) passes between the CROC and PENN GPS monuments, while CROC and CAPA lie on the hangingwall of the 09:40 fault (see Figs 3 and 4). This is fortunate for our modelling because the fit to the data measured in these monuments allows us to constrain the source model. In addition, the elevation changes at CROC and COLF are large enough to be included in the forward modelling (see Table 1). We note that the vertical coseismic displacements observed at the four closest sites are consistent with the pattern of vertical deformation resulting from SAR interferometry (Stramondo *et al.* 1999). In particular, this comparison confirms that only at CROC and COLF is it expected that vertical displacement measurements will be larger than GPS data uncertainties. This is a further corroboration of the data processing performed in this study.

**Table 3.** Horizontal and vertical coseismic displacements along the north (N), east (E) and vertical (U) components. The estimated accuracies ($2\sigma$) are reported in parentheses.

| Station | $N$ (m) | $E$ (m) | $U$ (m) |
|---|---|---|---|
| 01–COLF | −0.001 (±0.023) | 0.012 (±0.023) | −0.069 (±0.036) |
| 02–BEVA | 0.002 (±0.023) | 0.000 (±0.023) | −0.044 (±0.039) |
| 03–CROC | −0.138 (±0.023) | −0.019 (±0.023) | −0.247 (±0.042) |
| 04–CAPA | −0.057 (±0.023) | 0.011 (±0.023) | 0.001 (±0.039) |
| 05–CSAN | 0.024 (±0.025) | 0.001 (±0.025) | 0.012 (±0.046) |
| 06–FOLI | −0.032 (±0.023) | −0.032 (±0.023) | 0.033 (±0.037) |
| 07–GAIF | −0.007 (±0.023) | 0.036 (±0.023) | 0.017 (±0.040) |
| 08–OGAT | −0.008 (±0.023) | 0.037 (±0.023) | 0.040 (±0.036) |
| 09–PENN | 0.076 (±0.026) | 0.080 (±0.026) | −0.039 (±0.046) |
| 10–RIVO | −0.020 (±0.023) | −0.013 (±0.023) | −0.019 (±0.039) |
| 11–TPAR | 0.005 (±0.023) | −0.031 (±0.023) | −0.064 (±0.041) |
| 12–VISS | 0.027 (±0.025) | 0.008 (±0.025) | 0.023 (±0.045) |

We compute static displacements using a dislocation model in an elastic, homogeneous, isotropic half-space (see Okada 1985 and references therein). The fault is represented by a rectangular dislocation where slip distribution can be heterogeneous (see e.g. Arnadottir & Segall 1994; Hodgkinson *et al.* 1996). The source parameters of the dislocation model are the fault length, width, strike and dip, the depth of the top of the fault, and the strike and dip components of the slip vector. A heterogeneous slip distribution can be represented as a sum of several subsources distributed on the fault plane.

In the first set of tentative models we fix the strike and dip of the causative faults as well as the slip direction (rake angle) from the CMT solutions. We initially assume that the slip on the fault plane is uniform. In this way we attempt to constrain the fault length and width and the depth of the faults. In a second set of models, we verify the effect of changing the rake and we run a further set of models with a heterogeneous slip distribution for the 09:40 fault. In all these models, the possible range of variability for the input parameters is constrained with results and observations from other studies. We emphasize that this approach allows us to reduce the number of dislocation models that provide a reliable fit to the data. We briefly explain the constraints on fault geometry in this section.

The hypocentre locations are taken from Amato *et al.* (1998). The ruptures nucleated at shallow depths: the hypocentre of the first earthquake has been located at $6 \pm 1$ km and the second event at $6 \pm 2$ km (Massimo Di Bona, personal communication, 1998; see also Amato *et al.* 1998). The fault orientations and slip directions (strike, dip and rake) are taken from the CMT solutions obtained by Ekström *et al.* (1998), which show normal faulting with extension perpendicular to the Apennines. The distribution of aftershocks shows a NW–SE elongated fault zone extending for about 40 km (Amato *et al.* 1998), which is consistent with the orientation of ground and pavement ruptures induced by the two earthquakes (Cinti *et al.* 1999) and with the fault plane solutions of the main shocks and the largest aftershocks (Ekström *et al.* 1998). The 1997 main shocks did not produce any direct evidence of surface faulting (Cinti *et al.* 1999). The aftershock distribution reveals that the presumed fault planes dip SW, and that the rupture initiated close to the bottom edge of the activated fault planes (Ekström *et al.* 1998; Amato *et al.* 1998; Cinti *et al.* 1999). Table 4 lists the earthquake parameters for the largest events of the sequence from Ekström *et al.* (1998) and from standard CMT solutions. The seismic moments $M_o$ of the two shocks are $4.0 \times 10^{24}$ and $1.2 \times 10^{25}$ dyne cm.

The relative positions of the hypocentres of the two September 26 events (see Figs 1 and 2), the distribution of the early aftershocks (see Fig. 3 of Amato *et al.* 1998), the distribution of damage reported after each event (A. Tertulliani,

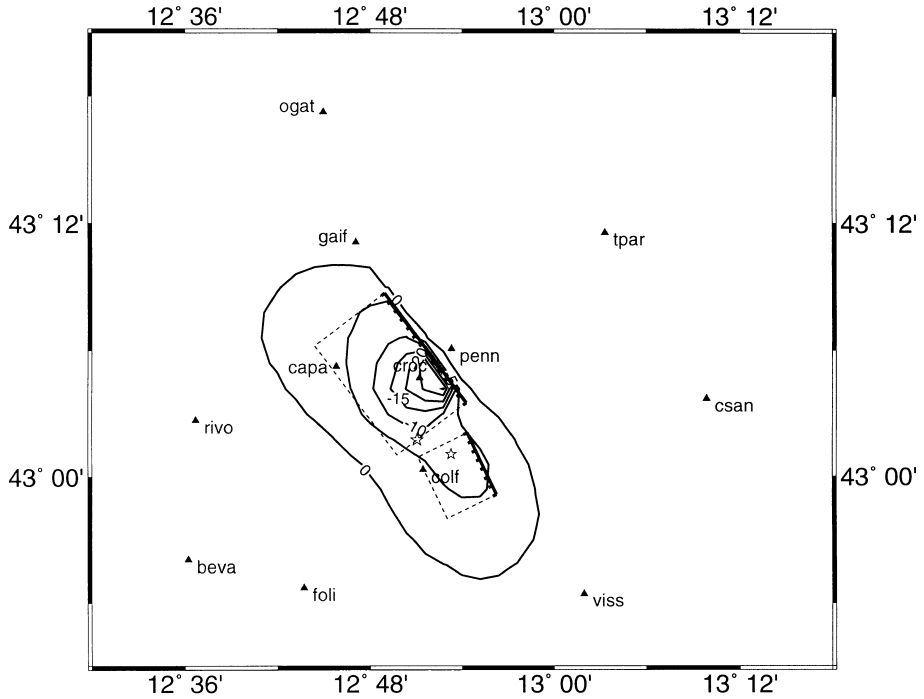


**Figure 4.** Contouring of vertical displacement (cm) predicted by the best-fitting model (see Table 5).

personal communication, 1997) and the distribution of peak ground acceleration (Berardi *et al.* 1998) all suggest that during the two earthquakes the rupture propagated in opposite directions along the same fault plane or on two adjacent parallel faults. This hypothesis agrees with the results of regional broad-band modelling performed by Pino *et al.* (1999) and with the analysis of strong motion data modelled by Zollo *et al.* (1998) and Capuano *et al.* (1999); these studies provide evidence for rupture directivity towards the SE for the 00:33 event and towards the NW for the 09:40 earthquake. Recent analysis of broad-band teleseismic data (Olivieri & Ekström 1999) as well as regional broad-band seismograms recorded by the MedNEt network (Pino *et al.* 1999) suggest that the 09:40 main shock is a complex event. Two subevents are evident in the source time functions, both associated with normal faulting. The first subevent ruptured towards the NW with a rupture duration of nearly 4.0 s, while the total source duration of the 09:40 earthquake was roughly 7.0 s; the 00:33 event had a rupture duration of nearly 5.0 s (Olivieri & Ekström 1999).

We use the seismic moment value and the source duration (assuming reasonable rupture velocities ranging between 2.5 and 3.0 km $s^{-1}$) to constrain the average slip and the source dimensions (length and width of the causative faults). According to the data and results discussed above, our starting model consists of two unilateral ruptures along distinct fault planes, the first rupturing towards the SE and the second towards the NW. For the first shock, we use fault lengths and widths ranging between 5 and 8 km; for the second event, we use fault lengths and widths ranging between 10 and 15 km and 7 and 10 km, respectively. The average slip changes with the fault dimension according to the seismic moment values. Although several observations and results suggest a unilateral rupture, we also consider a bilateral rupture as well as a unilateral rupture propagating in the opposite direction. We vary the fault depth as well as the position of the hypocentres on the fault plane, first with uniform dislocations, then with variable slip. We vary the dislocation only on the fault plane of the 09:40 earthquake, because it is more constrained by the available data than the 00:33 event.

## FORWARD MODELLING RESULTS

We will test the best fault geometries for the two earthquakes using all the available information from other investigations. We use in our modelling fault lengths and widths that match seismic moments and source durations with a reasonable rupture velocity. The first set of tentative models allowed us to verify that these constrained fault dimension values provide good initial models and an acceptable fit to the data. We will use a heterogeneous slip distribution only for the 09:40 earthquake, because the data do not permit us to constrain both fault geometry and slip distribution for the 00:33 fault.

The best fit to the data is obtained when the top of the fault of the 09:40 event is quite shallow, less than 1 km depth; if this fault is deeper, the fit in both amplitude and orientation of horizontal displacement vectors degrades. Fig. 5(a) shows the horizontal displacement residuals for both amplitude and orientation at CROC and PENN as a function of the upper fault depth. The orientation of the displacement vectors at all the monuments agrees better with the observations when the depth of the upper fault edge is shallower than 1.0 km and deeper than 0.3 km, but the fit to the amplitudes requires a fault shallower than 0.6 km. In particular, the fit of the horizontal displacement amplitude observed at PENN requires a quite shallow fault (see Fig. 5a): if the fault is deeper than 0.5 km the misfit becomes larger than the GPS data uncertainty. Furthermore, the fit of vertical displacement at CROC ($-24.7$ cm) also requires a shallow depth for the 09:40 fault plane. The fit of the vertical component at COLF and

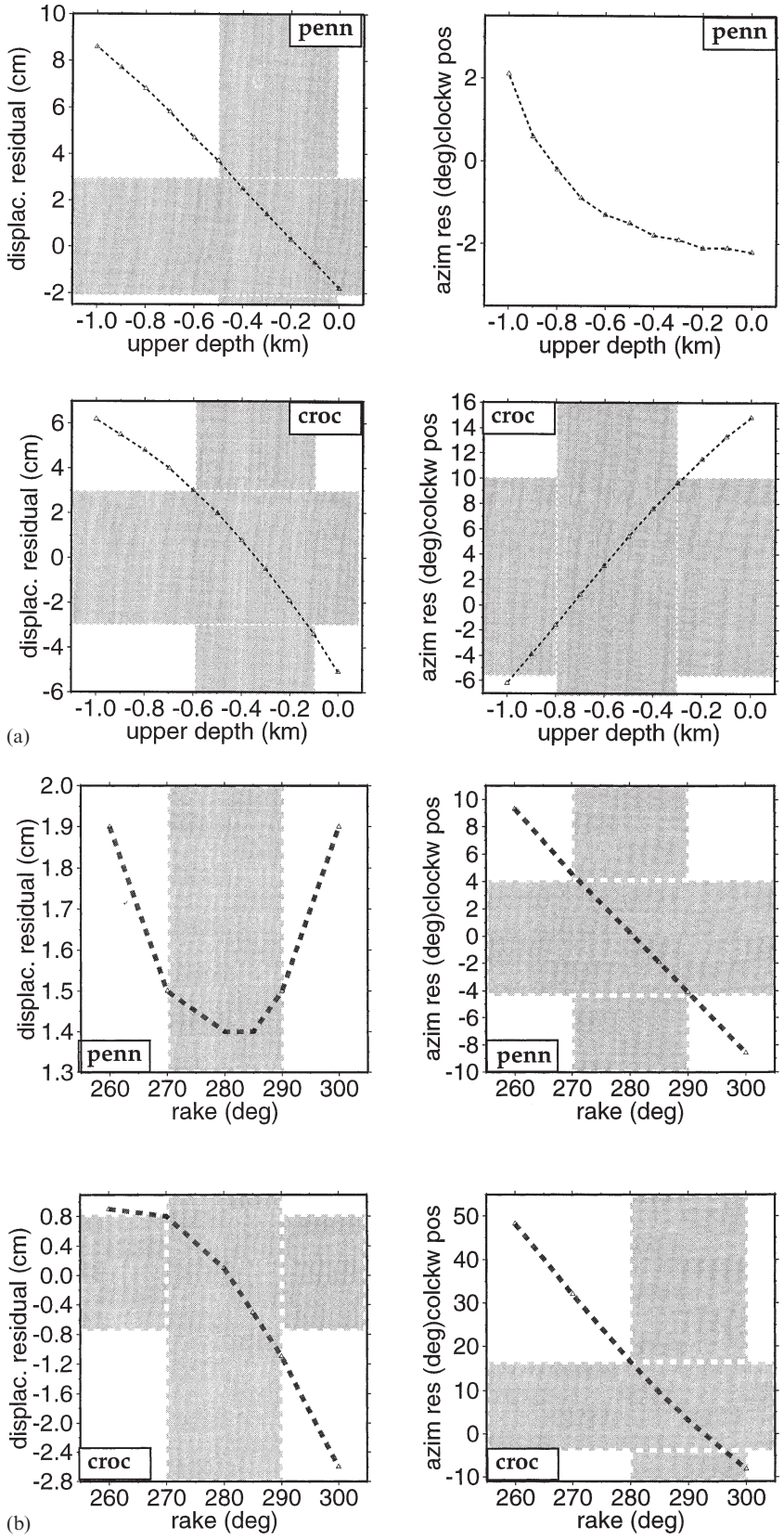


**Figure 5.** (a) Displacement residuals for both amplitude and orientation at PENN and CROC as a function of the upper depth of the 09:40 fault plane. (b) Displacement residuals as a function of the slip direction on the 09:40 fault plane.

**Table 4.** Earthquake parameters.

| Time (GMT) | Lat.* north | Long.* east | Depth* (km) | $M_0^{\diamond}$ (dyne cm) | $M_w^{\diamond}$ | Strike$^{\diamond}$ | Dip$^{\diamond}$ | Rake$^{\diamond}$ |
|---|---|---|---|---|---|---|---|---|
| 97/09/26 00:33 | 43°01′.31 | 12°53′.31 | $6\pm1$ | $0.40\times10^{25}$ | 5.67 | 152° | 46° | 277° |
| 97/09/26 00:33$^{+}$ | | | | $0.38\times10^{25}$ | 5.66 | 156° | 38° | 289° |
| 97/09/26 09:40 | 43°01′.77 | 12°51′.08 | $6\pm2$ | $1.20\times10^{25}$ | 5.99 | 144° | 42° | 280° |
| 97/09/26 09:40$^{+}$ | | | | $1.14\times10^{25}$ | 5.98 | 142° | 39° | 273° |
| 97/10/03 08:55 | 43°01′.88 | 12°50′.19 | $6.4\pm0.5$ | $0.86\times10^{24}$ | 5.20 | 141° | 43° | 286° |
| 97/10/06 23:24 | 43°01′.07 | 12°50′.33 | $7.1\pm0.6$ | $1.70\times10^{24}$ | 5.40 | 145° | 40° | 280° |
| 97/10/14 15:23 | 42°55′.15 | 12°55′.62 | $6\pm1$ | $0.34\times10^{25}$ | 5.62 | 122° | 38° | 260° |

* After Amato *et al.* (1998)
$^{\diamond}$ After Ekstrom *et al.* (1998)
$^{+}$ Standard CMT solution (Dziewonski *et al.* 1998)

the absence of horizontal displacement (less than the GPS uncertainty) suggest that the depth of the top edge of the 00:33 fault is deeper than 2.0 km.

We also investigate the influence of different slip directions on fitting the data. Fig. 5(b) shows the horizontal displacement residuals for both amplitude and orientation at CROC and PENN as a function of the rake angle. The best fit was obtained for rake angles ranging between 270° and 290°, which agrees well with the various CMT solutions (Table 4) and with the modelling results of Zollo *et al.* (1998) and Capuano *et al.* (1999). In particular, the horizontal displacements observed at CROC and CAPA (which are located on the hangingwall of the fault) constrain the slip direction. A pure normal fault solution provides an acceptable fit to the observed displacement amplitudes but the orientation residual at CROC and CAPA decreases for larger values of the rake angle. We have also tested the possibility of a bilateral rupture for both faults as well as of a unilateral rupture in the opposite direction (that is, the first event ruptured towards the NW while the second ruptured towards the SE). For both models the fit to the data is strongly degraded and misfits greatly increase. From these results we can exclude such alternative fault models.

A uniform slip model for the 09:40 fault does not allow one to fit both the horizontal and the vertical displacements at any of the three nearest sites, CROC, CAPA, and PENN. The simultaneous fit of these three sites requires an increase of slip in the SE section of the 09:40 fault. For this reason, we tried to fit the observations with a non-uniform slip distribution on the 09:40 fault plane. The resulting slip distribution for the best-fit model is shown in Fig. 6. Slip changes mostly along the fault strike, since the fit to the data observed at PENN and CROC requires large slip in the SE fault section (at shallow depth),

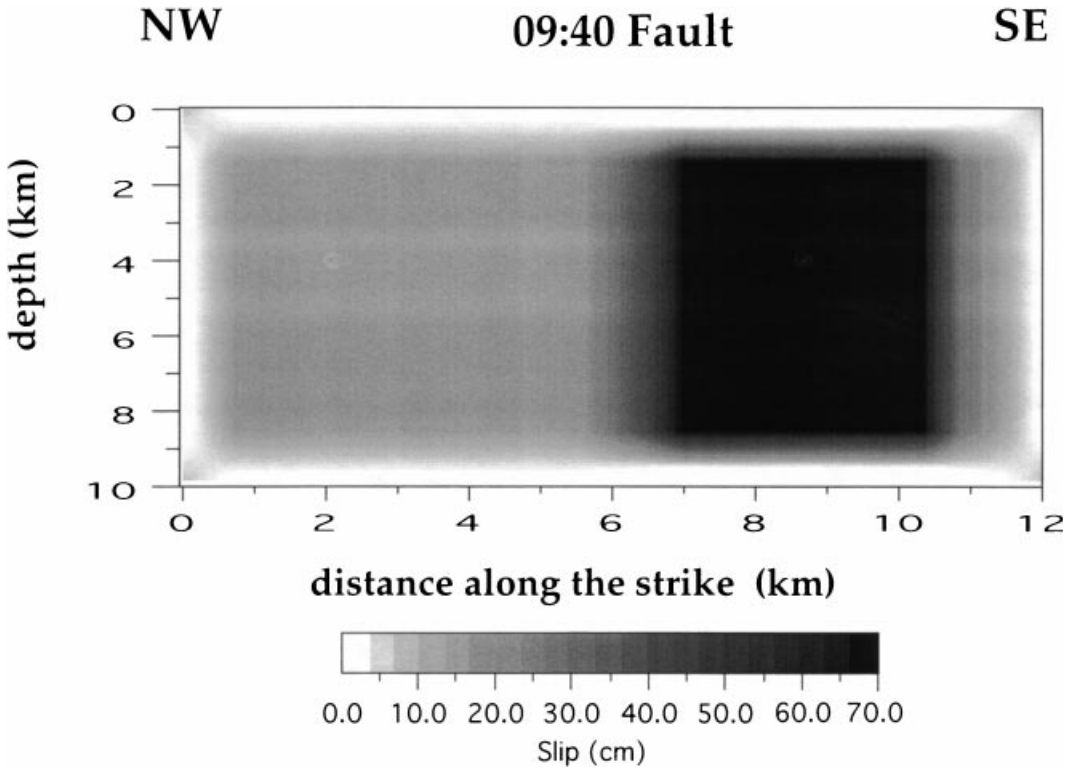


**Figure 6.** Slip distribution on the fault plane that ruptured during the 09:40 GMT earthquake of 1997 September 26 from the best-fitting model. Maximum slip on the plane is 65 cm (average value is 33 cm). The slip distribution on the 00:33 fault plane is kept uniform (see text).

while at CAPA we need slip on the deeper SE fault portion. Maximum slip on the 09:40 fault is 65 cm. An increase of slip in the NW fault section as well as a uniform slip model does not allow us to fit both amplitude and orientation of horizontal displacement at CAPA. For the 00:33 fault plane the depth, rather than a non-uniform slip distribution, strongly affects both the vertical and the horizontal fit at COLF, thus the slip on the 00:33 fault is held constant.

We summarize in the following the results of our forward modelling and we discuss the source parameters of the best-fitting model listed in Table 5 and shown in Fig. 6. Fig. 3 shows the comparison between model predictions and the horizontal observed displacements, while Fig. 4 shows the predicted vertical displacements. In Table 6 we compare the observed displacements and the model predictions resulting from the best-fitting model. We list only data from the sites for which measurements are well above the GPS data uncertainties (for either the horizontal or the vertical components). Our modelling results show that for the best-fitting model the upper depth of the fault is 0.5 km for the 09:40 event, while the depth of the top of the fault for the 00.33 event is not well constrained: values ranging between 3.8 and 2.4 km provide almost the same fit to the data (see Table 5). Among the numerous models tested in this study, our best-fitting model is the only one that allows us to retrieve 4 cm of subsidence at COLF (see Table 4).

The best-fitting model (Table 5 and Fig. 6) predicts horizontal displacements in good agreement with the observations at all the available monuments (see Table 6 and Fig. 3); the resulting misfit for the vertical component is quite satisfactory at both CROC and COLF, which are the only two monuments for which the observed vertical displacement is well above the GPS data uncertainties. Our best-fitting model predicts almost no vertical displacement at PENN. The observed vertical component at this site ($-3.9$ cm) is slightly above the GPS data uncertainty and below the threshold value we adopted in this study. Moreover, it is important to point out that a negative vertical displacement is incompatible with the observed amplitude of the horizontal displacement (11.0 cm). In fact, the amplitudes and orientations of the displacements observed at PENN and CROC strongly control the position of the surface projection of the fault and suggest that only CROC is on the fault hangingwall; therefore, the horizontal coseismic displacement at PENN is consistent only with a very small (positive) value of vertical displacement. The model prediction for the vertical displacement at COLF yields a misfit close to the observational error but still high (the residual is 2.8 cm), although it is the smallest residual amongst the numerous models tested in this study. Nevertheless, we believe that the best-fitting model proposed in this study is well constrained both by GPS data and by results from other investigations.

In order to verify the reliability of the dislocation model proposed to fit the horizontal and vertical GPS displacements, we compare in Fig. 7 the resulting vertical displacement pattern (shown in Fig. 4) with the surface deformation pattern resulting from SAR interferometry (Stramondo *et al.* 1999). Fig. 7 indicates that the best-fitting model (Table 5) proposed in this study guarantees an acceptable fit to an independent data set: the area of maximum subsidence observed in the SAR interferogram is quite well reproduced by our best-fitting model. We emphasize that the result of this comparison confirms the absence of measurable vertical deformation at PENN. We believe that these results provide an important validation of the proposed model.

## POSSIBLE CONTRIBUTIONS FROM OTHER EARTHQUAKES

The 1997 post-earthquake GPS survey was performed between October 7 and 11. Two moderate-magnitude earthquakes occurred between the earthquakes of September 26 investigated in this study and the GPS campaign, on October 3 at 08:55 GMT, $M_w$ 5.2, and on October 6 at 23:24 GMT, $M_w$ 5.4, both located close to the 09:40 GMT hypocentre

**Table 5.** Model parameters of the best-fitting model.

| Event | $M_0$ (dyne cm) | Strike | Dip | Rake | $L$ (km) | $W$ (km) | $D$ (cm) | $z_t^a$ (km) |
|---|---|---|---|---|---|---|---|---|
| 97/09/26 00:33 | $4.5\times10^{24}$ | 154° | 46° | 283° | 6 | 7 | 36 | 2.4 |
| 97/09/26 09:40 | $1.2\times10^{25}$ | 143° | 40° | 285° | 12 | 10 | 33[b] | 0.5 |

[a] Depth of the top edge of the fault
[b] Average value

**Table 6.** Measured and modelled displacement resulting from best-fitting model (two faults).

| Station | Horizontal Observed (cm) | Horizontal Predicted (cm) | Horizontal Misfit (cm) | Vertical Observed (cm) | Vertical Predicted (cm) | Vertical Misfit (cm) |
|---|---|---|---|---|---|---|
| CROC | 14 | 14 | 0 | −25 | −27 | 2 |
| CAPA | 6 | 4 | 2 | 1[a] | −3 | – |
| PENN | 11 | 10 | 1 | −3.9[a] | 1 | – |
| COLF | 1[a] | 2 | – | −7 | −4 | −3 |
| FOLI | 4 | 2 | 2 | 3[a] | 0 | – |

[a] Data are less than GPS uncertainties

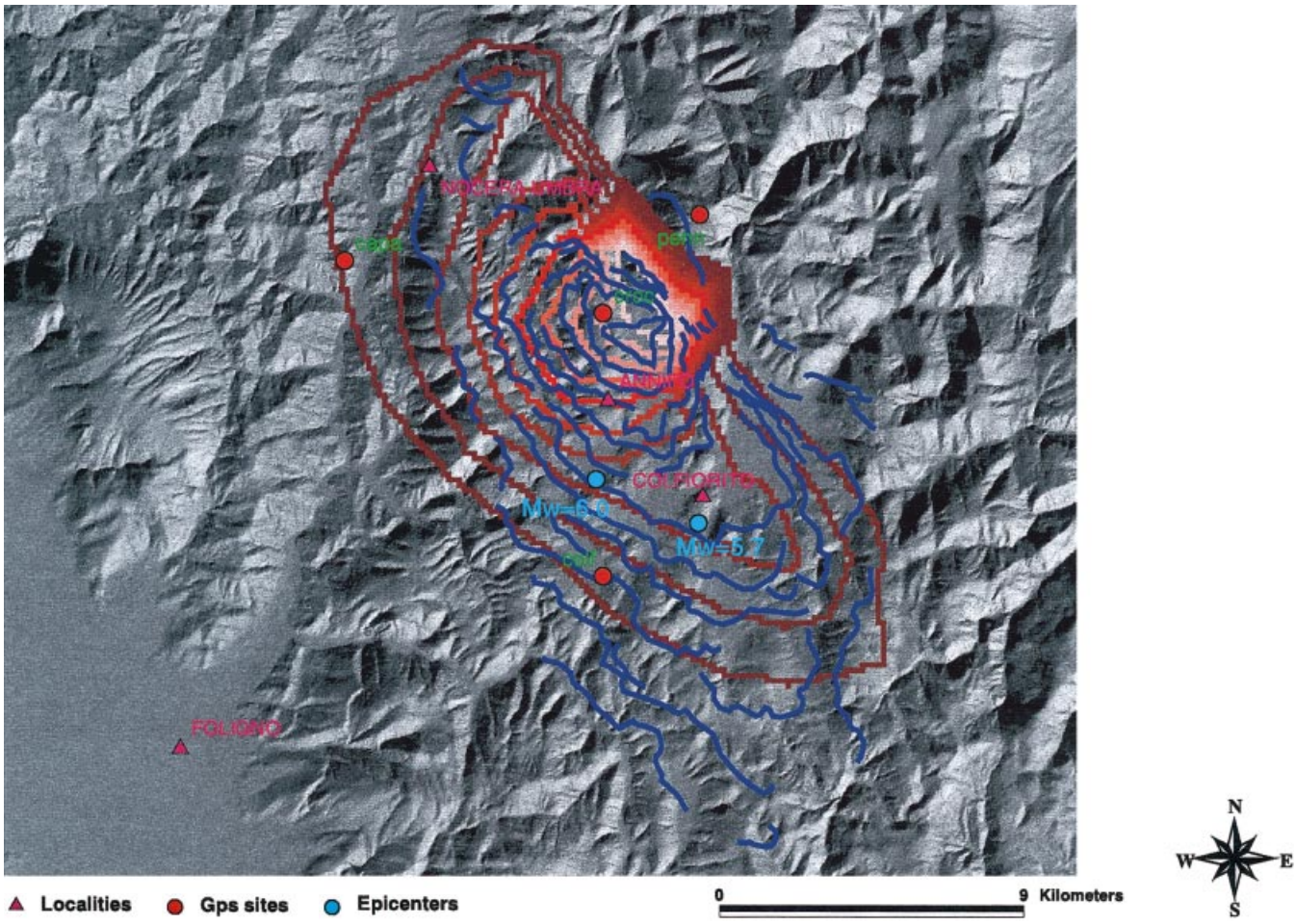


**Figure 7.** Comparison between the pattern of vertical displacement simulated using the best-fitting model (red lines) and the vertical deformation pattern resulting from SAR interferometry (blue lines). Line separation is 5 cm. The positions of the closest GPS monuments (red solid circles) and the topography of the area are also shown on the map (redrawn from Stramondo *et al.* 1999). Blue solid circles show the epicentres of the two main shocks of September 26; triangles show the two main cities of the area, which were severely damaged.

(see Fig. 1), between CROC and COLF. Fault plane solutions (Ekström *et al.* 1998) and good-quality hypocentre locations (Amato *et al.* 1998) are available for these events (see Fig. 1 and Table 4). Even if we cannot constrain in detail the fault geometries of these two events, they could have contributed to the observed surface deformation. In this section we tentatively test this hypothesis. The two October events have similar focal mechanisms and they were located very close to each other. The suggested fault models are listed in Table 7. Source parameters of the 00:33 and 09:40 faults are those previously discussed (best-fitting model), except that the slip on the 00:33 fault is now 27 cm. Figs 8 and 9 show the horizontal and vertical displacements predicted using the four-faults model (see also Table 8). This model improves the fit to the data observed at FOLI and COLF (see Table 6). We conclude that these two events contributed slightly to the observed vertical displacements, increasing the area that underwent subsidence (see Figs 4 and 9). A value of nearly 5 cm of subsidence at COLF agrees with the vertical deformation resulting from SAR interferograms (Stramondo *et al.* 1999). With the four-faults model, uniform slip for the 09:40 event does not allow us to fit the observed GPS displacements at PENN and CROC,

**Table 7.** Model parameters for the four-faults model.

| Event | $M_0$ (dyne cm) | Strike | Dip | Rake | $L$ (km) | $W$ (km) | $D$ (cm) | $z_t^a$ (km) |
|---|---|---|---|---|---|---|---|---|
| 97/09/26 00:33 | $3.4\times10^{24}$ | 154° | 46° | 283° | 6 | 7 | 27 | 2.4 |
| 97/09/26 09:40 | $1.2\times10^{25}$ | 143° | 40° | 285° | 12 | 10 | 33[b] | 0.5 |
| 97/10/03 08:55 | $8.6\times10^{23}$ | 141° | 43° | 286° | 4 | 4 | 18 | 3.0 |
| 97/10/06 23:24 | $1.7\times10^{24}$ | 145° | 40° | 280° | 5 | 5 | 23 | 3.2 |

[a] Depth of the top edge of the fault
[b] Average value

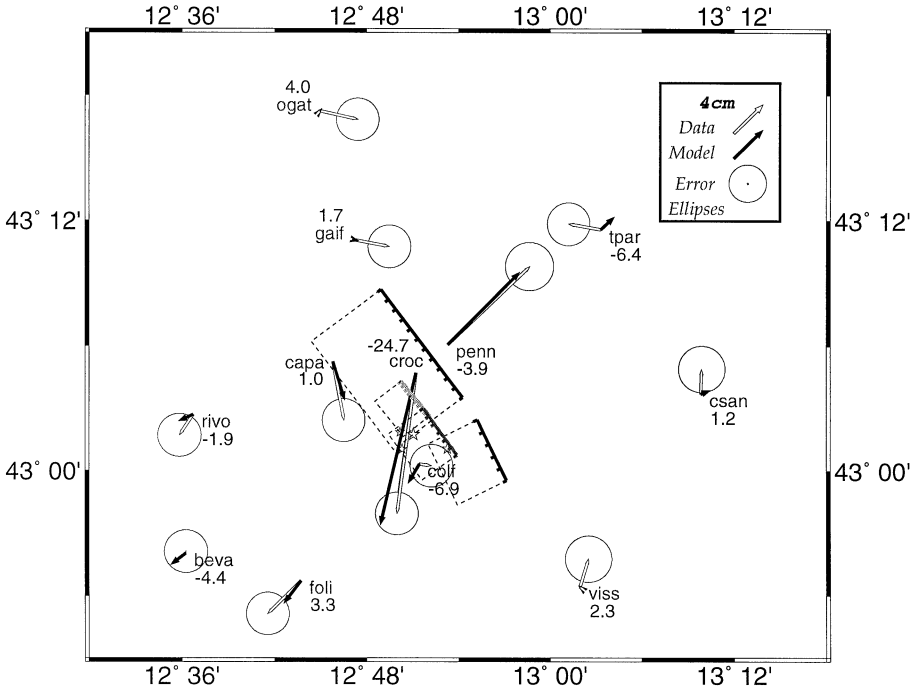


**Figure 8.** Comparison between observed GPS horizontal displacements (open arrows) and predicted displacements (solid arrows) using the four-faults model for the two September 26 and the October 3 and 6 earthquakes. The epicentres (stars) of the four earthquakes and the error ellipses of the two GPS campaigns are shown. The surface projections of the activated faults are shown as a line with ticks on the downthrown side.

confirming the best-fitting model listed in Table 5 and shown in Fig. 6. According to the four-faults model the fault depth of the 00:33 event can be shallower than 3 km. Our modelling results do not permit us to constrain a fixed value for the 00:33 fault depth: values ranging between 1.7 and 3.8 km fit the observed GPS displacements satisfactorily.

## CONCLUSIONS

We fitted vertical and horizontal coseismic displacements resulting from GPS measurements in order to propose a dislocation model for the two earthquakes that occurred on 1997 September 26 at 00:33 and 09:40 GMT in the central

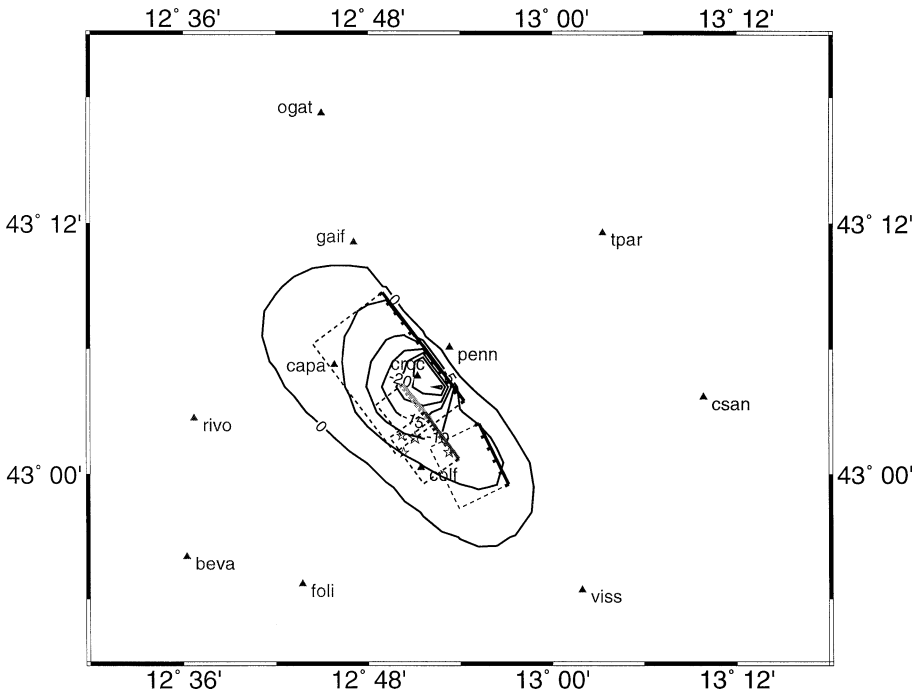


**Figure 9.** Contouring of vertical displacement (cm) predicted by the four-faults model.

**Table 8.** Measured and modelled displacements for the four-faults model.

| Station | Horizontal Observed (cm) | Horizontal Predicted (cm) | Horizontal Misfit (cm) | Vertical Observed (cm) | Vertical Predicted (cm) | Vertical Misfit (cm) |
|---|---|---|---|---|---|---|
| CROC | 14 | 15 | −1 | −25 | −28 | 3 |
| CAPA | 6 | 4 | 2 | 1[a] | −4 | – |
| PENN | 11 | 10 | 1 | −3.9[a] | 1 | – |
| COLF | 1[a] | 2 | – | −7 | −5 | −2 |
| FOLI | 4 | 3 | 1 | 3[a] | 0 | – |

[a] Data are less than GPS uncertainties

Apennines (Umbria–Marche). Despite the small dimension of the available data set, the position of the GPS monuments with respect to the activated faults and the availability of the seismological data permitted us to propose a sufficiently well-constrained source model that is consistent with the observations and the results arising from other investigations (Amato *et al.* 1998; Ekström *et al.* 1998; Cinti *et al.* 1999; Olivieri & Ekström 1999; Pino *et al.* 1999).

The source parameters of the best-fitting model are listed in Table 5 and the fit to the data is shown in Figs 3, 4 and 7 and listed in Table 6. Based on the fit to the data, we can exclude a bilateral rupture as well as a unilateral rupture in the opposite direction. Fault lengths and widths are quite well constrained and allow us to match seismic moments and rupture durations (Ekström *et al.* 1998; Olivieri & Ekström 1999). The slip distribution for the 09:40 event is not uniform, as shown in Fig. 6. Our best-fitting model is very consistent with the rupture model proposed by Capuano *et al.* (1999), who modelled strong-motion data. It provides a good fit to the vertical displacement pattern resulting from SAR interferometry (see Fig. 7 and Stramondo *et al.* 1999). The agreement between models resulting from independent data sets further confirms the reliability of our results.

We have verified that two smaller-magnitude earthquakes that occurred on October 3 at 08:55 ($M_w$ 5.2) and October 6 at 23:24 ($M_w$ 5.4) (both located close to the 09:40 earthquake) contributed slightly to the observed coseismic displacements. These two events enlarged the area of subsidence. Modelling results confirm that the 00:33 fault plane is deeper than the 09:40 fault plane; the former has to be deeper than 1.7 km. We obtained an acceptable fit using a fault depth of 2.4 km for the 00.33 fault. We note that the four-faults model allows the 00:33 fault plane to be shallower than that resulting from the best-fitting model discussed in the previous section. This result is more consistent with the distribution of main shocks and aftershocks at depth (Amato *et al.* 1998), which shows that large-magnitude earthquakes nucleated at the bottom of the seismogenic layer. We emphasize that geodetic data represent an important tool to constrain dislocation models for the moderate-magnitude earthquakes of the 1997 Umbria–Marche sequence. Geodetic observations resulting from GPS and SAR analyses have to be considered in order to interpret surface geological data.

## ACKNOWLEDGMENTS

We are grateful to L. Surace and the IGMI for providing us with the data from their 1992–1996 campaign, which motivated and allowed this study. We thank ENEL (Italian Electric Company) for offering us logistic support during the campaign. We also thank S. Del Mese and M. Vecchi for help in fieldwork. We thank S. Salvi and S. Stramondo, who provided the processed DinSAR interferogram. We benefitted from useful discussions with G. Selvaggi, S. Salvi, C. Chiarabba, S. Stramondo and F. Cinti. We thank P. England, H. G. Kahle, R. Stein, A. Amato and an anonymous referee for their helpful revision of the manuscript and Enzo Boschi for his encouragement during this study. This research was partially funded by the Italian Space Agency.

## REFERENCES

Amato, A. *et al.*, 1998. The 1997 Umbria-Marche, Central Italy, earthquake sequence: a first look at main shocks and aftershocks, *Geophys. Res. Lett.,* **25,** 2861–2864.

Arnadottir, T. & Segall, P., 1994. The 1989 Loma Prieta earthquake imaged from inversion of geodetic data, *J. geophys. Res.,* **99,** 835–855.

Berardi, R. *et al.*, 1998. Strong ground motion during the 1997 Umbria-Marche earthquake sequence, *EGS Annual Conference, Nice, France* (abstract).

Bernard, P. & Zollo, A., 1989. The Irpinia (Italy) 1980 earthquake: detailed analysis of a complex normal fault, *J. geophys. Res.,* **94,** 1631–1648.

Boschi, E., Ferrari, G., Gasperini, P., Guidoboni, E., Smriglio, G. & Valensise, G., 1995. *Catalogo dei forti terremoti in Italia dal 461 a.C. al 1980,* Pubblicazione dell'Istituto Nazionale di Geofisica, Rome.

Capuano, P., De Natale, G., Gasparini, P., Pingue, F. & Scarpa, R., 1988. A model for the 1908 Messina Straits (Italy) earthquake by inversion of levelling data, *Bull. seism. Soc. Am.,* **78,** 1930–1947.

Capuano P., Zollo, A., Emolo, A., Marcucci, S. & Milana, G., 1999. Rupture mechanism and source parameters of the Umbria-Marche mainshocks from strong motion data, *J. Seism.,* in press.

Cinti, F., Cucci, L., Marra, F. & Montone, P., 1999. The Umbria-Marche (Italy) sequence: relationship between ground deformation and seismogenic structure, *Geophys. Res. Lett.,* **26,** 893–898.

De Natale, G. & Pingue, F., 1991. A variable slip fault model for the 1908 Messina Straits (Italy) earthquake, by inversion of levelling data, *Geophys. J. Int.,* **104,** 73–84.

Deschamps, A., Iannaccone, G. & Scarpa, R., 1984. The Umbrian earthquake (Italy) of 19 September 1979, *Ann. Geophys.,* **2,** 29–36.

Ekström, G., Morelli, A., Dziewonski, A.M., & Boschi, E., 1998. Moment tensor analysis of the Umbria-Marche earthquake sequence of September-October 1997, *Geophys. Res. Lett.,* **25,** 1971–1974.

Haessler, H. *et al.*, 1988. The Perugia (Italy) earthquake of 29 April 1984: a microearthquake survey, *Bull. seism. Soc. Am.,* **78,** 1948–1964.

Hodgkinson, K.M., Stein, R.S. & Marshall, G., 1996. Geometry of the 1954 Fairview Peak-Dixie Valley earthquake sequence from a joint inversion of leveling and triangulation data, *J. geophys. Res.,* **101,** 25 437–25 457.

Hunstad, I. & England, P.C., 1999. Geodetic strain of central and southern Italy from repeated triangulation in the interval 1860–1965, *Earth planet. Sci. Lett.*, **169,** 261–267.

Okada, Y., 1985. Surface deformation due to shear and tensile faults in a half-space, *Bull. seism. Soc. Am.,* **75,** 1135–1154.

Olivieri, M. & Ekström, G., 1999. Rupture depths and source processes of the 1997–1998 earthquake sequence in central Italy, *Bull. seism. Soc. Am.,* **89,** 305–310.

Pantosti, D. & Valensise, G., 1990. Faulting mechanism and complexity of the 23 November, 1980, Campania-Lucania earthquake inferred from surface observations, *J. geophys. Res.,* **95,** 15 319–15 341.

Pingue, F. & De Natale, G., 1993. Fault mechanism of the 40 seconds subevent of the 1980 Irpinia (southern Italy) earthquake from levelling data, *Geophys. Res. Lett.,* **20,** 911–914.

Pino, N.A., Mazza, S. & Boschi, E., 1999. Rupture directivity of the major shocks in the 1997 Umbria-Marche (Central Italy) sequence from regional broadband waveforms, *Geophys. Res. Lett.,* **26,** 2101–2104.

Rothacher, M. & Mervart, L., 1996. *Bernese GPS Software Version 4.0,* Astronomical Institute, University of Berne.

Stramondo, S. *et al.*, 1999. The September 26, 1997 Central Italy earthquakes: coseismic surface displacement detected by SAR interferometry and GPS, and faulting modeling, *Geophys. Res. Lett.,* **26,** 883–886.

Surace, L., 1993. Il progetto IGM95, *Boll. Geod. Sci. Affini,* **3,** 219–230.

Surace, L., 1997. La nuova rete geodetica nazionale IGM95: risultati e prospettive di utilizzazione, *Boll. Geod. Sci. Affini,* **3,** 357–378.

Ward, S.N. & Valensise, G., 1989. Fault parameters and slip distribution of the 1915, Avezzano, Italy earthquake derived from geodetic observations, *Bull. seism. Soc. Am.,* **79,** 690–710.

Zollo, A., Marcucci, S., Milana, G., Bongiovanni, G., Capuano, P., Emolo, A. & Herrero, A., 1998. The 1997 Colfiorito earthquake sequence (central Italy): insights on the mainshock ruptures from near source strong motion records, *EGS Annual Conference, Nice, France* (abstract).